Research Square

Preprints are preliminary reports that have not undergone peer review.
They should not be considered conclusive, used to inform clinical practice,
or referenced by the media as validated information.

Loss of NDUFB10 disrupts respirasome formation and reduces in situ cytochrome c oxidase function

Nico Marx
University of Münster
Marie-Theres Borowski
University of Münster
Tasnim Arroum
University of Münster
Karin B. Busch
buschkar@uni-muenster.de

University of Münster

Article

Keywords: Mitochondrial respiratory chain, respiratory supercomplexes, complex I deficiency, cytochrome c oxidase, NDUFB10

Posted Date: November 24th, 2026

DOI: https://doi.org/10.21203/rs.3.rs-11695198/v1

License: This work is licensed under a Creative Commons Attribution 4.0 International License.
Read Full License

Additional Declarations: No competing interests reported.

Abstract

Respiratory complex I (CI) deficiency disrupts mitochondrial supercomplex assembly, impacting bioenergetics in diseases like Parkinson's and Leigh Syndrome. The role of CI subunit NDUFB10 in complex IV (CIV) assembly and activity remains unclear. Here we generated NDUFB10 knockout human cells to analyze respiratory supercomplex composition and CIV function. Loss of NDUFB10 abolished CI-containing respirasomes, increased III_2/IV subcomplexes stabilized by enhanced SCAF1 binding, and reduced CIV activity measured in permeabilized cells, leading to decreased mitochondrial ATP production. However, isolated CIV enzymatic assays showed no significant activity difference, indicating that CIV performance depends on its native supercomplex context. These findings suggest that optimal mitochondrial respiration relies on cooperative organization of respiratory complexes within supercomplexes, highlighting the importance of CI integrity for CIV function in situ.

Introduction

The mitochondrial respiratory chain consists of four complexes (CI–CIV): NADH-ubiquinone oxidoreductase (complex I, CI), succinate dehydrogenase (complex II, CII), ubiquinol-cytochrome c oxidoreductase (complex III, CIII), and cytochrome c oxidase (complex IV, CIV). CI, CIII, and CIV can further oligomerize into supercomplexes (SCs): N-respirasomes (I + III_2+IV) and Q-respirasomes (III_2+IV) [1]. Recent cryo-electron tomography has revealed additional compositions across species [2–10], which are supported by functional evidence [11–15]. SC assembly primarily stabilizes its constituent complexes, potentially improving electron transport efficiency and limiting ROS production [11, 14, 16, 17]. However, the functional advantages of SCs are still debated [14, 18, 19]. Because the stoichiometries of CI, CIII, and CIV, as well as the mobile carriers, are unequal [20], not all complexes are found in supercomplexes. Consequently, CIV and CIII mainly exist in smaller complexes, such as III_2/IV Q-respirasomes, alongside to I/III_2/IV supercomplexes. In OXPHOS-dependent tissues, such as neurons, CI exists almost exclusively within SCs, whereas glycolytic astrocytes also contain free CI, which correlates with elevated ROS [21]. CI is essential for SC assembly [17], and the P-membrane module (composed of P_{P-a}, P_{P-b}, P_{D-a} and P_{D-b} segments) [22, 23] seems critical for SC assembly [24]. As we and others have recently shown [22, 25], loss of NDUFB10, a subunit of the P module, prevents CI assembly and the formation I_1/III_2/IV N-respirasomes. Building the III_2/IV Q-respirasomes requires the SC assembly factor SCAF1 (COX7A2L) [12, 26–28], though it appears to be dispensable for N-respirasomes [28]. N-respirasomes can instead incorporate the isoform COX7A2 [29, 30]. The two respirasome types differ structurally and bioenergetically: SCAF1-containing respirasomes adopt a tighter conformation, exhibit higher NADH-dependent respiration, and produce lower levels of ROS [12]. This seems to be another indication that respirasome formation has functional consequences for the electron transport chain. To investigate this further, we used of the CI-deficient system, in which no N-respirasomes form, to study the activity of the respiratory complexes, particularly CIV, *in situ*. We observed an increase in III_2/IV when CI was not assembled. Furthermore, more SCAF1 was bound to III_2/IV, suggesting a stabilizing function. However, the CIV activity, as tested by different approaches, was significantly

reduced. This suggests that CIV function may be influenced by its cooperation with CI and CIII in the N-respirasome.

Results

Loss of CI-supercomplexes results in increase of $CIII_2$/CIV subcomplexes stabilized through SCAF1 binding

As we and others previously have shown, knockout of NDUFB10, a subunit of complex I, results in loss of I+III_2+IV supercomplexes in HAP cells [22, 25]. NDUFB10 is part of the P_D-$_a$ module and required for stable assembly of CI [22]. Loss of CI-supercomplexes was accompanied by an increase in III_2+IV subcomplexes but SCAF1 expression was downregulated. This finding was surprising, since SCAF1, also known as COX7A2L, is required for III_2+IV assembly and stability [31]. In zebrafish, its loss disrupted III_2+IV and III_2+IV_2 supercomplexes and altered OXPHOS activity [32]. We therefore determined SCAF1 protein expression levels and SCAF1 binding to CIII and CIV by Blue native gel electrophoretic separation of complexes and supercomplexes and subsequent immune-staining. As reported before, in NDUFB10-KO, CI containing supercomplexes were completely abolished, while the SCAF1-signal indicated stronger binding to the III_2+IV supercomplex and to co-migrating III/IV_2 complexes (Fig. 1a). Additionally, in contrast to wildtype, no free SCAF1 signal was detected. Overall, SCAF1 protein levels decreased as revealed by WESTERN-blotting (Fig. 1a,b). We suggest that, in NDUFB10-KO cells, free SCAF1 is recruited to III_2+IV stabilizing their interaction in spite of the reduction in the overall level of SCAF1 mRNA [25] and protein (Fig. 1b).

Loss of respirasome supercomplex formation compromises Complex IV activity

We wondered, whether loss of the N-respirasome and shift towards stabilized III_2+IV has an effect on the complex IV activity. To test for this, we run different assays starting with *in situ* measurement of cytochrome *c* oxidase activity via oxygen consumption measurements in permeabilized cells supplied with substrates for CI, CII and CIV (Fig. 2a). The activity of CIV after supplying CI substrate was essentially absent in NDUFB10-KO cells. Also, when CII substrate was supplied, the knock-out cells exhibited significant reduction of oxygen-consumption indicating that CII activity could not compensate for loss of CI activity. Finally, when CIV activity was measured by application of ascorbate and TMPD, known substrates for CIV, the significant reduced activity of cytochrome *c* oxidase per se revealed that CIV activity itself was the cause of reduced respiration (Fig. 2b). To test cytochrome *c* oxidation function of CIV directly, we isolated mitochondria and added reduced cytochrome *c.* We found reduced cytochrome *c* oxidation kinetics of isolated mitochondria from NDUFB10-knockout cells in a similar range as after KCN inhibition of CIV (Fig. 2c). In addition, we performed a coupled in-gel activity assay of cytochrome *c* oxidase activity supplying reduced cytochrome *c*. As expected, no CIV activity was

detected where usually N-respirasomes are found, instead, we found CIV activity in several lower molecular weight bands that indicate in III_2+IV, IV_2 and IV. In a rescue cell line, CIV activity in N-respirasomes was reinstalled (Fig. 2c). The CIV activity bands showed no difference in intensity, since this was an end-point measurement after 16 h of incubation.

Finally, we conducted a CIV activity assay using solubilized CIV from isolated mitochondria. Cytochrome *c* from cow heart (30 µM) was added and oxygen consumption rate was measured with a Clark-type oxygen electrode (Oxygraph+, Hansatech; Pentney, UK) at 25°C with 20 mM ascorbate as the electron donor. OCR is reported as nmol O_2*min^{-1}*mg^{-1} protein. In average, complex IV activity was lower in NDUFB10-KO cells (85%), but due to the high variance, the difference was not significant ($p \sim 0.22$) (Table 1). Since this measurement was performed using dissolved CIV, its natural environment within the cristae had been largely disrupted, which might affect the activity.

Table 1
Cox activity in wildtype, NDUFB10-KO and rescue conditions

Average turnover rate [nmol O_2*min^{-1}*mg^{-1} protein]	**wildtype**	**NDUFB10-KO**	**Rescue**
	2.68	**2.27**	**2.39**
SD	0.76	0.66	0.42
n	10	8	12
StER	0.24	0.23	0.12
%	100	85	89

Discussion

We recently showed that knockout of the P_{D-a} subunit NDUFB10 of CI resulted in incomplete assembly of CI, loss of the respirasome and increase of III_2/IV supercomplex. Here, we demonstrate that this is based on increased SCAF1 binding to III_2/IV. SCAF1 is essential for the assembly of III_2/IV: it attaches to incomplete CIII and builds a docking station for CIV [31, 33], but as it remains in the supercomplex and keeps it together, it is a bona fide subunit [34, 35]. Interestingly, SCAF1 was recruited from the free SCAF1 pool, which got depleted in NDUFB10 knockout, to the supercomplex. We next tested, how the loss of I/III_2/IV and shift towards more III_2/IV assemblies would affect electron transport and CIV activity. Data from Cryo-EM structure and kinetics in yeast suggest that the III_2/IV supercomplex facilitates surface diffusion of cytochrome c in 2D, providing an advantage to 3D diffusion between free III_2 and IV [36]. Stabilization of III_2/IV by SCAF1 may help maintain respiration in the remaining supercomplex when respirasome formation is impaired due to incomplete CI assembly. This dynamic remodeling of respirasome architecture through recruitment of SCAF1 is consistent with the plasticity model of supercomplex organization [11, 18]. The decreased ROS formation in NDUFB10-knockout also could be explained by optimized coupling of CIII and CIV in III_2/IV.

To test this, we determined oxygen consumption rates (OCR) in permeabilized HAP wildtype and NDUFB10-knockout cells. We supplied substrate for CI, but due to its deficiency, no respiration was detected. With substrate for CII, OCR was still significantly reduced. Finally, we supplied CIV directly with substrate and still found a CIV activity level reduced by half compared to the wildtype, indicating that CIV activity itself was hampered (Fig. 2a). To test this further, we isolated mitochondria from wildtype and CI-deficient cells and determined cytochrome *c* oxidation rates after supply with reduced cytochrome *c*. The cytochrome c oxidation rate was significantly reduced in NDUFB10-knockout cells supporting compromised CIV activity (Fig. 2b). Next, we checked in-gel-cytochrome *c* oxidation activity of CIV in native gels. All forms of CIV (III_2/IV, IV_2, and IV) were active demonstrating that the capacity of CIV for cytochrome c oxidation was not affected in NDUFB10-KO (Fig. 2c). This was confirmed by an assay, where we used solubilized CIV from isolated mitochondria to measure oxygen-consumption after cytochrome c - H_2 supply (Table 1). Together, the data show that the activity rate of CIV in the native environment (Fig. 2a-b) was reduced in CI-compromised cells, despite an upregulation and stabilization of III_2/IV. CIV, which had been removed from its native environment (Fig. 2c-d), still showed full capacity under optimal conditions of substrate supply. This suggests that the increased and more stable assembly of CIV in III_2/IV could not compensate for the loss of the respirasome, which further suggests that the organization of CIV in I/III_2/IV matters for overall optimal activity of CIV. Since CIV, next to adenine nucleotide translocator and ATP synthase (CV) [37], is the kinetic bottleneck in respiration, its activtiy is relevant for electron flow rates. Consequently, losing optimal I/III_2/IV nano-assembly is associated with impaired in situ CIV performance and ATP synthesis, suggesting that mitochondrial energy output may depend on cooperative inter-complex organization rather than the isolated capacity of individual enzymes [26].. CV expression levels did not change in the NDUFB10-knockout system, which reduces the likelihood that a feed-back mechanism impeded CIV activity. Rather, our data suggest a functional advantage of CIV assembly in respirasomes to optimize electron transport chain kinetics *in situ*.

Methods

All methods were carried out in accordance with relevant guidelines and regulations.

Cell cultivation

HAP1 parental wildtype (WT) and NDUFB10 knockout cells were purchased from Horizon Discovery (Horizon Genomics GmbH). The cells were cultivated in IMDM at 37°C and 5% carbon dioxide. The knockout of NDUFB10 in HAP cells (Figure S1) was generated using Safe Harbor, clustered regularly interspaced short palindromic repeats (CRISPR)/ CRISPR-associated protein 9 (Cas9) and homology-directed repair (HDR). A plasmid containing the CRISPR/Cas9 and homologous flanks to NDUFB10 was introduced into a Safe Harbor. The target gene, NDUFB10, was cut by CRISPR/Cas9, and with a template not including NDUFB10, the double-strand break was repaired via HDR as previously described [25].

Immunostaining

The membrane was washed with 1x TBS-T and incubated in 10% milk in 1x TBS-T for 1 hour at room

temperature. The primary antibody NDUFB10 and others were diluted (dilutions see Table 2) in 1% milk in 1x TBS-T and incubated overnight at 4°C under shaking. As a normalization

Table 2
List of used primary and secondary antibodies.

Primary antibody	**Manufacturer**	**Host organism**	**Dilution**
beta actin	Sigma (A1978)	mouse	1:5000
Cox8A	St. Johns Laboratory (STJ26230)	rabbit	1:500
GFP	Thermo Fischer (MA5-15256)	mouse	1:1000
NDUFB10	Abcam (MS604-300)	rabbit	1:5000
NDUFS3	Abcam (ab183733)	rabbit	1:2000
SDHA	Abcam (Ab14715)	mouse	1:2000
Secondary antibody			
Goat anti-mouse IgG H&L	Biozol (LIN-ITC207P)		1:2000
Goat anti-rabbit	Biozol (LIN-ITC208P)		1:2000

the primary antibody anti-Beta Actin was used. The secondary antibody was diluted 1:2000 in 1% milk and the membrane was incubated with this dilution for 1 hour at room temperature. The secondary antibody was then discarded, and the membrane was washed three times with TBS-T. For imaging, the membranes were incubated in 1:1 ECL for 5 minutes. Chemiluminescence was measured using a fluorometer.

Respiration measurements

The activities of the individual respiratory chain complexes in Hap cells were determined using a Seahorse XFe96 Analyzer via membrane permeabilization and sequential addition of specific substrates and inhibitors. One day before experiment, 20,000 to 30,000 cells per well were seeded into a Seahorse XF cell culture microplate and incubated at 37°C and 5% CO_2, while the sensor cartridge was calibrated overnight with XF Calibrant at 37°C. Prior to the measurement, cells were washed once with MAS^{++} buffer and then 180 µl of prewarmed MAS^{++} buffer (pH 7.4) was added. This buffer permeabilizes the membranes via 0.0006% digitonin and, in addition to the 1x MAS base buffer (660 mM mannitol, 210 mM sucrose, 30 mM KH_2PO_4, 6 mM HEPES, 3 mM EGTA, 15 mM $MgCl_2$) already contains 0.5 µM of the uncoupler FCCP as well as 10 mM glutamate and 10 mM malate for the initial stimulation of CI. The

actual measurement of the OCR was performed at 37°C. To isolate the specific activities of the remaining respiratory chain complexes, a sequential injection was performed:

- Port A: Injection of a final concentration of 0.5 µM rotenone to inhibit CI.
- Port B: Injection of final concentrations of the CII substrates succinate (10 mM) and glycerol-3-phosphate (5 mM).
- Port C: Injection of a final concentration of 0.5 µM antimycin A to inhibit CIII.
- Port D: Injection of final concentrations TMPD (100 µM) and ascorbate (10 mM), which allows for the isolated measurement of CIV activity.

With the final injection, cells were stained with Hoechst 33342 (2 µg/ml) for counting them with the Cytation 5 for normalization to cell number.

Isolation of mitochondria

For isolation of mitochondria from cultured mammalian cells, ~ 23 × 10^6 cells were harvested and cell pellets were frozen at − 80°C. All following procedures were performed on ice. The cell pellet was briefly thawed and recentrifuged at 300 × g for 5 min at 4°C. The supernatant was discarded and the pellet was resuspended in mitochondria isolation buffer (MIB) (0.32 M sucrose, 1 mM EDTA, and 10 mM Tris–HCl, pH 7.4). For mechanical destruction, the cell suspension was transferred into a Dounce homogenizer (B.Braun). The cell lysates were centrifuged at 800 × g for 5 min at 4°C. This step was repeated until no cell pellet was visible any more. Finally, the supernatant was centrifuged at 10,000 × g for 10 min at 4°C followed by resuspension of the pellet in mitochondrial isolation buffer and concentration quantification.

Enzyme activity assays

1. CIV activity (spectrophotometry)

Isolated mitochondria were frozen at − 80°C, thawed on ice, resuspended briefly and refrozen to disrupt the mitochondrial membrane.

For the Complex IV activity assay, first 10mg/ml Cytochrome c was reduced in MiliQ using sodium ditionine for 4h on ice covered from light and pH was adjusted to 7.2. Assays were performed in 96 well plates in 10mM potassium phosphate buffer containing 1mg/ml reduced cytochrome c with 20 µg of isolated mitochondria per well. The optical density (OD) was measured in 10 s intervals using a Cytation 5 (Agilent) in the kinetic readout mode.

Oxidation of Cytochrome c was measured at OD 550 for 2 min at 30°C and addition of CIV inhibitor 1mM KCN was used as a positive control for reaction specificity.

1. CIV activity (Clark-electrode)

Protein concentration of the isolated mitochondria was determined with the DC protein assay kit (Bio-Rad). For each measurement, 10 µg of total mitochondrial protein were resuspended in COX solubilization buffer (10 mM K-HEPES, pH 7.4, 40 mM KCl, 1% Tween 20, 1 mM phenylmethylsulfonyl fluoride, 1 mM heat-activated sodium vanadate, 10 mM KF, 2 mM EGTA), and mitochondrial membranes were disrupted by sonication (Sonic Dismembrator Model 100, Fisher Scientific, Waltham, MA, USA, three 5 s pulses). Oxygen consumption was measured continuously with a Clark-type oxygen electrode (Oxygraph+, Hansatech Instruments, Pentney, UK) at 25°C in the presence of 20 mM ascorbate and 30 µM cow heart cytochrome *c* (Sigma, C3131). Data were analyzed with OxyTrace+ software (version 1.0 Build 48, Hansatech Instruments).

1. CIV in-gel activity

CIV in-gel activity was assessed after BN-PAGE as described [38]. The gel was incubated in 10 mL of CIV activity buffer (50 mM phosphate buffer, pH 7.4, 0.5 mg/mL 3,3'-diaminobenzidine tetrahydrochloride (DAB, Sigma, D5637), 1 mg/mL cytochrome *c* (Sigma, C3131)).

Mitochondrial ROS measurements

Mitochondrial superoxide levels were quantified using the fluorogenic probe MitoSOX Red (Life Technologies M36008), with MitoTracker Green (MTG, Invitrogen M7514) co-staining applied to normalize the signal against total mitochondrial mass. Cells were incubated with 2.5 µM MitoSOX Red and 100 nM MTG for 30 min at 37°C under a 5% CO_2. Following three washes with dye-free medium, live-cell imaging was performed in medium supplemented with 2.5 µM MitoSOX Red using a Leica TCS SP8 SMD confocal microscope (63x water objective, HC PL APO 63x/1.20 W motCorr CS2) equipped with a live-cell incubation chamber (37°C, 5% CO_2). Fluorescence excitation was achieved using a white light laser (WLL) at 488 nm for MTG and 561 nm for MitoSOX Red. Emission signals were recorded via hybrid detectors (HyDs) at 498–549 nm and 660–779 nm, respectively. Integrated density signals per cell were quantified in Fiji/ImageJ (v1.53), and final ROS levels were expressed as the relative MitoSOX/MTG ratio.

Declarations

Competing Interest Statement

No competing interest are to be declared.

Funding:

The project was funded by an HFSP project (RGP0016/2018).

Author Contribution

N.M., T.A., M.T.B. and K.B. designed the study. N.M., T.A., M.T.B. conducted activity assays. N.M., T.A., M.T.B. and K.B analyzed physiological and molecular biology data. N.M., M.T.B. and K.B. wrote the manuscript. All authors reviewed the manuscript.

Acknowledgement

We would like to thank Frank Schmelter for technical assistance.

Data Availability

Source gel data are provided in the Supplementary data set file.

References

1. Schagger, H. & Pfeiffer, K. Supercomplexes in the respiratory chains of yeast and mammalian mitochondria. *EMBO J.* **19** (8), 1777–1783 (2000).
2. Guo, R., Zong, S., Wu, M., Gu, J. & Yang, M. *Architecture of Human Mitochondrial Respiratory Megacomplex I(2)III(2)IV(2).*Cell, 170(6): pp. 1247–1257 e12. (2017).
3. Letts, J. A., Fiedorczuk, K., Degliesposti, G., Skehel, M. & Sazanov, L. A. Structures of Respiratory Supercomplex I + III(2) Reveal Functional and Conformational Crosstalk. *Mol. Cell.* **75** (6), 1131–1146e6 (2019).
4. Muhleip, A. et al. Structural basis of mitochondrial membrane bending by the I-II-III(2)-IV(2) supercomplex. *Nature* **615** (7954), 934–938 (2023).
5. Nakano, A. et al. *Structures of respiratory supercomplexes and ATP synthase oligomers in mammalian mitochondrial inner membrane*. *Nat. Commun.*, **17**(1). (2026).
6. Waltz, F. et al. *In-cell Archit. mitochondrial respiratory chain Sci.*, **387**(6740): 1296–1301. (2025).
7. Wu, M., Gu, J., Guo, R., Huang, Y. & Yang, M. *Structure of Mammalian Respiratory Supercomplex I(1)III(2)IV(1).*Cell, 167(6): pp. 1598–1609 e10. (2016).
8. Zheng, W., Chai, P., Zhu, J. & Zhang, K. High-resolution in situ structures of mammalian respiratory supercomplexes. *Nature* **631** (8019), 232–239 (2024).
9. Sousa, J. S., Mills, D. J., Vonck, J. & Kuhlbrandt, W. *Functional asymmetry and electron flow in the bovine respirasome*. *Elife*, 5. (2016).
10. Dudkina, N. V., Kudryashev, M., Stahlberg, H. & Boekema, E. J. Interaction of complexes I, III, and IV within the bovine respirasome by single particle cryoelectron tomography. *Proc. Natl. Acad. Sci. U S A.* **108** (37), 15196–15200 (2011).

11. Acin-Perez, R. & Enriquez, J. A. The function of the respiratory supercomplexes: the plasticity model. *Biochim. Biophys. Acta*. **1837** (4), 444–450 (2014).
12. Calvo, E. et al. Functional role of respiratory supercomplexes in mice: SCAF1 relevance and segmentation of the Q(pool). *Sci. Adv.* **6** (26), eaba7509 (2020).
13. Berndtsson, J. et al. Respiratory supercomplexes enhance electron transport by decreasing cytochrome c diffusion distance. *EMBO Rep.* **21** (12), e51015 (2020).
14. Barrientos, A. & Ugalde, C. I function, therefore I am: overcoming skepticism about mitochondrial supercomplexes. *Cell. Metab.* **18** (2), 147–149 (2013).
15. Liang, C. et al. *Formation of I(2) + III(2) supercomplex rescues respiratory chain defects.*Cell Metab, (2025).
16. Maranzana, E., Barbero, G., Falasca, A. I., Lenaz, G. & Genova, M. L. Mitochondrial respiratory supercomplex association limits production of reactive oxygen species from complex I. *Antioxid. Redox Signal.* **19** (13), 1469–1480 (2013).
17. Moreno-Lastres, D. et al. Mitochondrial complex I plays an essential role in human respirasome assembly. *Cell. Metab.* **15** (3), 324–335 (2012).
18. Milenkovic, D. et al. Preserved respiratory chain capacity and physiology in mice with profoundly reduced levels of mitochondrial respirasomes. *Cell. Metab.* **35** (10), 1799–1813 (2023). e7.
19. Letts, J. A., Fiedorczuk, K. & Sazanov, L. A. The architecture of respiratory supercomplexes. *Nature* **537** (7622), 644–648 (2016).
20. Schwerzmann, K., Cruz-Orive, L. M., Eggman, R., Sanger, A. & Weibel, E. R. Molecular architecture of the inner membrane of mitochondria from rat liver: a combined biochemical and stereological study. *J. Cell. Biol.* **102** (1), 97–103 (1986).
21. Lopez-Fabuel, I. et al. Complex I assembly into supercomplexes determines differential mitochondrial ROS production in neurons and astrocytes. *Proc. Natl. Acad. Sci. U S A*. **113** (46), 13063–13068 (2016).
22. Stroud, D. A. et al. Accessory subunits are integral for assembly and function of human mitochondrial complex I. *Nature* **538** (7623), 123–126 (2016).
23. Guerrero-Castillo, S. et al. *The Assembly Pathw. Mitochondrial Respiratory Chain Complex. I Cell. Metab.*, **25**(1): 128–139. (2017).
24. Fang, H. et al. A membrane arm of mitochondrial complex I sufficient to promote respirasome formation. *Cell. Rep.* **35** (2), 108963 (2021).
25. Arroum, T. et al. Loss of respiratory complex I subunit NDUFB10 affects complex I assembly and supercomplex formation. *Biol. Chem.* **404** (5), 399–415 (2023).
26. Lapuente-Brun, E. et al. *Supercomplex assembly determines electron. flux mitochondrial electron. Transp. chain Sci.*, **340**(6140): 1567–1570. (2013).
27. Lobo-Jarne, T. & Ugalde, C. Respiratory chain supercomplexes: Structures, function and biogenesis. *Semin Cell. Dev. Biol.* **76**, 179–190 (2018).

28. Perez-Perez, R. et al. COX7A2L Is a Mitochondrial Complex III Binding Protein that Stabilizes the III2 + IV Supercomplex without Affecting Respirasome Formation. *Cell. Rep.* **16** (9), 2387–2398 (2016).
29. Fernandez-Vizarra, E. et al. Two independent respiratory chains adapt OXPHOS performance to glycolytic switch. *Cell. Metab.* **34** (11), 1792–1808 (2022). e6.
30. Zong, S. et al. Structure of the intact 14-subunit human cytochrome c oxidase. *Cell. Res.* **28** (10), 1026–1034 (2018).
31. Cogliati, S. et al. Mechanism of super-assembly of respiratory complexes III and IV. *Nature* **539** (7630), 579–582 (2016).
32. Garcia-Poyatos, C. et al. Scaf1 promotes respiratory supercomplexes and metabolic efficiency in zebrafish. *EMBO Rep.* **21** (7), e50287 (2020).
33. Lobo-Jarne, T. et al. Human COX7A2L Regulates Complex III Biogenesis and Promotes Supercomplex Organization Remodeling without Affecting Mitochondrial Bioenergetics. *Cell. Rep.* **25** (7), 1786–1799e4 (2018).
34. Vercellino, I. & Sazanov, L. A. The assembly, regulation and function of the mitochondrial respiratory chain. *Nat. Rev. Mol. Cell. Biol.* **23** (2), 141–161 (2022).
35. Vercellino, I. & Sazanov, L. A. Structure and assembly of the mammalian mitochondrial supercomplex CIII(2)CIV. *Nature* **598** (7880), 364–367 (2021).
36. Moe, A., Di Trani, J., Rubinstein, J. L. & Brzezinski, P. *Cryo-EM structure and kinetics reveal electron transfer by 2D diffusion of cytochrome c in the yeast III-IV respiratory supercomplex* Vol. 118 (Proc Natl Acad Sci U S A, 2021). 11.
37. Groen, A. K., Wanders, R. J. A., Westerhoff, H. V., Vandermeer, R. & Tager, J. M. Quantification of the Contribution of Various Steps to the Control of Mitochondrial Respiration. *J. Biol. Chem.* **257** (6), 2754–2757 (1982).
38. Jha, P., Wang, X. & Auwerx, J. Analysis of Mitochondrial Respiratory Chain Supercomplexes Using Blue Native Polyacrylamide Gel Electrophoresis (BN-PAGE). *Curr. Protoc. Mouse Biol.* **6** (1), 1–14 (2016).

Figures

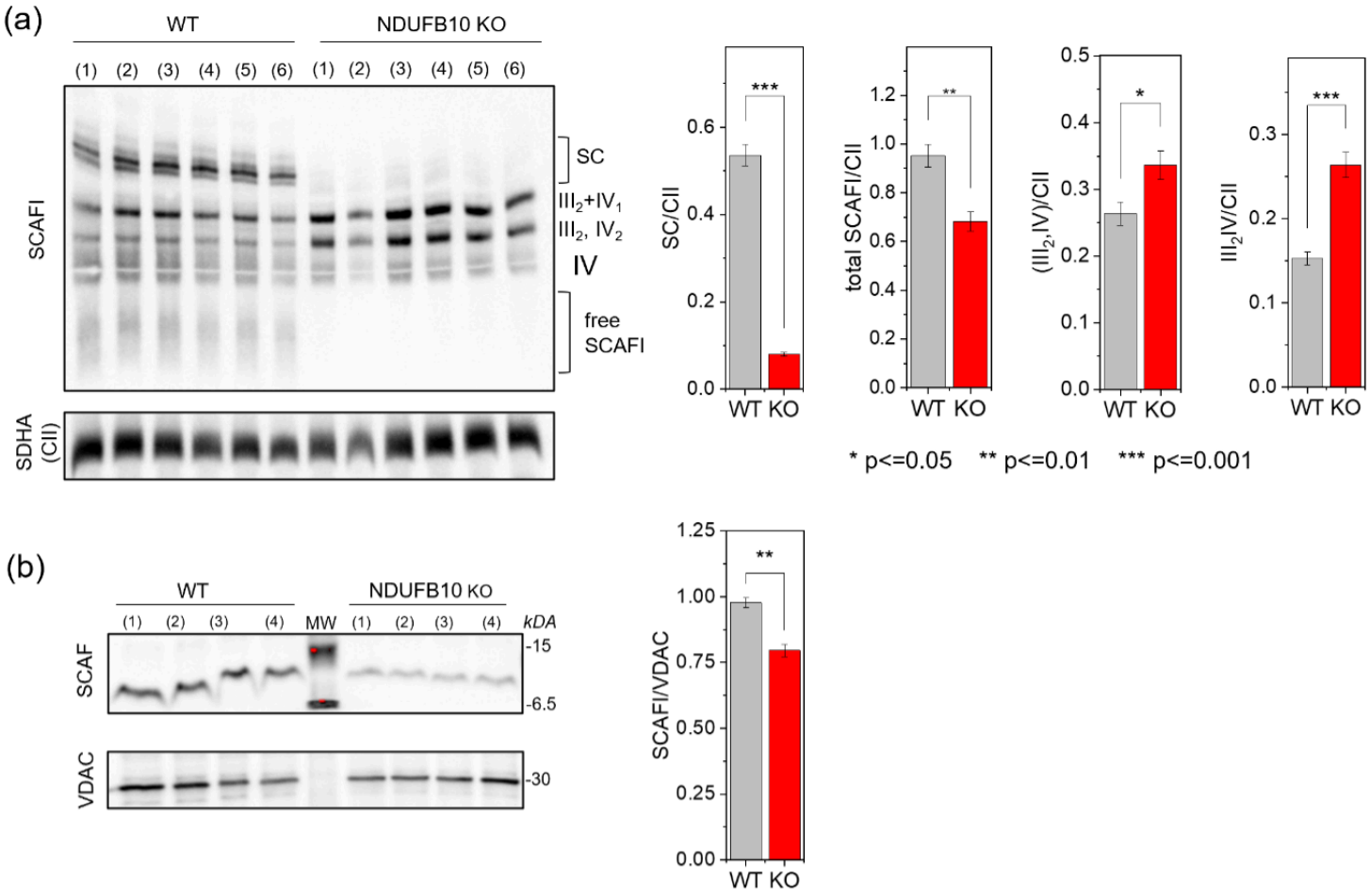

Figure 1

SCAF1 binding stabilizes CIII2/CIV complexes in CI-deficient NDUFB10 knockout cells. (a) *Blue native gel (BN)-PAGE separated proteins immune-blotted against SCAF1 and quantification of binding normalized to SDHA (same blot), a CII subunit. 6 preparations of control and NDFUB10-KO cells.* ***(b)*** *SCAF1-protein levels in wildtype and NDUFB10-KO cells. SDS-PAGE and immunostaining of SCAF1 and VDAC.*

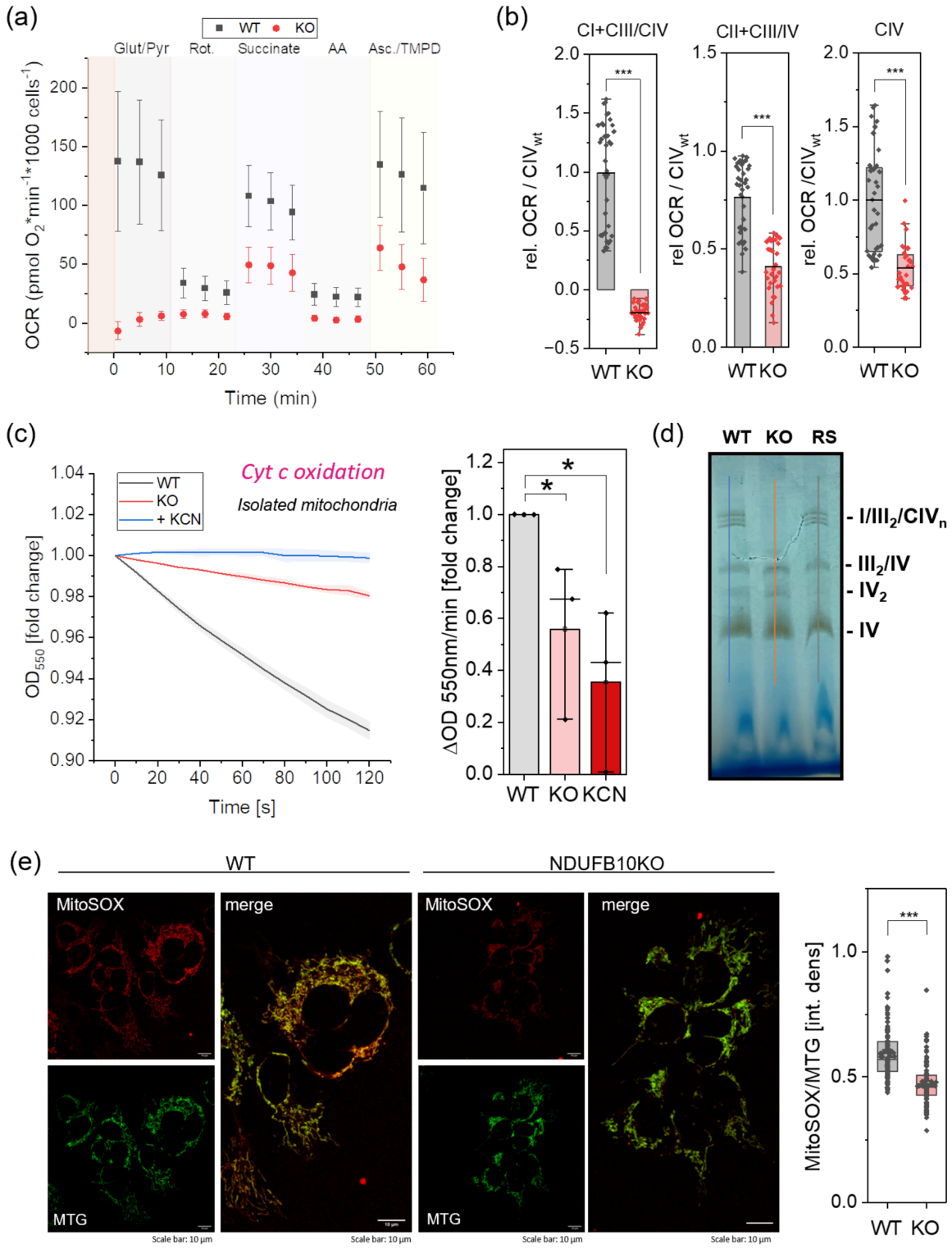

Figure 2

Effects of SC loss on complex IV activity. (a) Oxygen Consumption Measurements (OCR) of control and NDUFB10-KO HAP cells to determine complex activities. Cells were permeabilized before substrate and inhibitor application. (b) N-respirasome (CI+CIII/CIV) activity under substrate saturation (glutamate/pyruvate). Activity of Q-respirasome with electrons deriving from CII (CII+CIII/CIV) after inhibition of CI by rotenone and substrate application for CII (succinate), and complex IV activity (CIV)

tested via ascorbate oxidation. (c) CIV activity in isolated mitochondria determined via cytochrome c oxidase activity. (d) In-gel activity of CIV measured as a cytochrome c oxidation in a coupled assays running for 16 hours resulting in DAB precipitation.

Supplementary Files

This is a list of supplementary files associated with this preprint. Click to download.

- Sourcedatagels.pdf